Numerical modelling and quantification of coastal urban compound flooding

Yuan, Jiao; Zheng, Feifei; Duan, Huan Feng; Deng, Zhengzhi; Kapelan, Zoran; Savic, Dragan; Shao, Tan; Huang, Wei Min; Zhao, Tongtiegang; Chen, Xiaohong

DOI
10.1016/j.jhydrol.2024.130716

Publication date
2024

Document Version
Final published version

Published in
Journal of Hydrology

Journal of Hydrology 630 (2024) 130716

Contents lists available at ScienceDirect

Journal of Hydrology

journal homepage: www.elsevier.com/locate/jhydrol

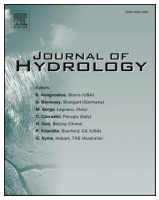

Research papers

Numerical modelling and quantification of coastal urban compound flooding

Jiao Yuan [a], Feifei Zheng [a,*], Huan-Feng Duan [b], Zhengzhi Deng [c], Zoran Kapelan [d], Dragan Savic [e,f,g], Tan Shao [h], Wei-Min Huang [h], Tongtiegang Zhao [i], Xiaohong Chen [i]

[a] College of Civil Engineering and Architecture, Zhejiang University, Hangzhou 310058, China
[b] Department of Civil and Environmental Engineering, The Hong Kong Polytechnic University, Hung Hom, Kowloon, Hong Kong Special Administrative Region
[c] Ocean College, Zhejiang University, Zhoushan 316000, China
[d] Delft University of Technology, Department of Water Management, Delft, The Netherlands
[e] KWR Water Research Institute, Nieuwegein, The Netherlands
[f] University of Exeter, Exeter, United Kingdom
[g] Faculty of Civil Engineering, University of Belgrade, Serbia
[h] Hydrological Measurement & Report Center at Zhuhai City, Guangdong Hydrological Bureau, Zhuhai 519000, China
[i] Center for Water Resources and Environment, School of Civil Engineering, Sun Yat-sen University, Guangzhou 510275, China

ARTICLE INFO

This manuscript was handled by Y. Huang, Editor-in-Chief, with the assistance of Habib Basha, Associate Editor

Keywords:
Compound flooding
Complex river network
Numerical modelling
Scenario analysis

ABSTRACT

Low-lying coastal cities are vulnerable to compound floods caused by many factors including river flows, tides and local rainfall. Many previous studies focus on the impacts of rainfall and tidal levels (two driving factors) on estuaries or regions near the main single river, while research about the three influencing factors on the floods for complex urban river networks remain relatively scarce. This paper proposes a framework to simulate the coastal compound flooding process, with a series of scenarios designed to explore the main flooding drivers and their worst possible combination. The approach is used to quantify the induced flooding consequences, in which a two-dimensional model is employed to conduct a case study for a city with complex river networks. The Qianshan River basin in Zhuhai City, located in the Guangdong-Hong Kong-Macao Greater Bay Area (GBA) of China is used as the case study. Application results show that: (i) the occurrence and properties of flooding in this coastal area are jointly affected by upstream river flows, downstream tidal levels and local rainfall intensity with different contribution levels, (ii) compared to tidal levels, local rainfall intensity has a larger impact on the flooding levels of the study region, and (iii) the worst scenario where a 50-year return period upstream river flow co-occurring with high tide and a 100-year return period rainfall can produce a flooding area up to 50 km^2 for the study region, with an average of 1.3 m flooded depth. The proposed framework with its findings offers an in-depth understanding and quantification of coastal urban flood characteristics within the GBA of China.

1. Introduction

In recent years, due to rapid urbanization and global climate change, flooding has become one of the most challenging problems globally (Dash and Punia, 2019; Li et al., 2019). For instance, according to the statistical analysis of 40 years between 1970 and 2019, around 44 % of the global meteorological disasters are related to floods, resulting in 58,700 deaths, accounting for 31 % of total economic losses caused by the top ten disasters (WMO, 2021; Gran Castro and Ramos De Robles, 2019). On a worldwide scale, coastal-river areas are often attractive for population gathering, urban infrastructure development and economic activities (Bermudez et al., 2021). As pointed out in the United Nations report, 40 % of the world's population is living in coastal areas on different continents (UNRIC, 2022). For example, low-altitude coastal areas in China only account for 2 % of the country's land, but have more than 12 % of the country's population (Fang et al., 2021). Therefore, flooding in these coastal cities can lead to serious consequences.

The physical process of flooding in coastal cities can be complex as it is vulnerable to the compound effects of multiple driving factors, such as heavy rainfall, high tidal levels and high river flows (Lian et al., 2017).

* Corresponding author.
E-mail addresses: yuanjiao@zju.edu.cn (J. Yuan), feifeizheng@zju.edu.cn (F. Zheng), hf.duan@polyu.edu.hk (H.-F. Duan), zzdeng@zju.edu.cn (Z. Deng), Z.Kapelan@tudelft.nl (Z. Kapelan), Dragan.Savic@kwrwater.nl (D. Savic), zhaottg@mail.sysu.edu.cn (T. Shao), eescxh@mail.sysu.edu.cn (W.-M. Huang).

https://doi.org/10.1016/j.jhydrol.2024.130716
Received 13 October 2023; Received in revised form 16 November 2023; Accepted 26 November 2023
Available online 23 January 2024

Wahl et al. (2015), Zscheischler et al. (2018) and Moftakhari et al (2017) have emphasized that compound flooding in coastal cities caused simultaneously by multiple factors is often more serious than floods caused by rainstorms or high tidal levels alone. In this regard, the floods in Ravenna, Italy (Bevacqua et al., 2017) and Hurricane Harvey floods in Houston (Valle-Levinson et al., 2020) confirmed this finding. Therefore, it is necessary to consider the correlation and interaction of compound driving factors when studying coastal urban flooding (Bevacqua et al., 2020; Couasnon et al., 2020).

To address this issue, many studies have been conducted over the past decade, which can be classified into two main categories. The first category is to describe the correlation between different driving factors or their joint distribution using statistical models (Jane et al., 2020). For example, Ward et al. (2018) and Bevacqua et al. (2020) confirmed the strong correlation between high sea levels and high river flows observed in global deltas and estuaries based on observation data and prediction models; Zheng et al. (2013) and Wahl et al. (2015) analyzed the joint probability of rainfall and tidal levels at Australian and American coastal cities; Moftakhari et al. (2017) developed a statistical model to estimate the joint return period of river flow and coastal water level; Eilander et al. (2020) focused on the correlation analysis between rainfall and river flow for many different coastal cities. These studies show that, for low-lying coastal areas, flooding can be usually caused by extreme rainfall, river flow and high tidal levels, and the compound effects of the three factors can result in more serious consequences (Moftakhari et al., 2019).

The second category of existing studies is to simulate the complex physical processes through numerical models in order to explore the comprehensive impacts of driving factors on compound floods (Shen et al., 2019). Hydrodynamic models have an advantage in considering the hydraulic characteristics of coastal urban drainage systems, river networks, streets and other micro topography (Qi et al., 2021). When considering rainfall and runoff processes in flood simulation, hydrological models and surface overflow models are often jointly used. For example, Chen et al. (2018) combined the one-dimensional drainage system model with a two-dimensional diffusion surface flow model to simulate floods in the Haidian island of China.

A large number of studies have used storm surge models such as Delft3D (Kumbier et al., 2018) , ADCIRC (Bilskie and Hagen, 2018), FVCOM (Nakamura et al., 2019) and SCHISM (Liu et al., 2020) to assess coastal flood risk. For example, Rey et al. (2020) used a high-resolution model to study the comprehensive impact of wind field and rainfall on flood and circulation in coastal estuaries. Zhang et al. (2020) evaluated the compound flood impact of storm tide, rainfall and river overflow on the southern coast of Caribbean Island countries through a simplified two-dimensional hydrodynamic model. Most of these studies select estuarine areas or river mainstream for simulation, while Lian et al. (2013) and Shi et al. (2022) have constructed the hydrodynamic models of river networks in Fuzhou and Hangzhou respectively. However, Lian (2013) did not simulate surface overflow as it only represented the severity of flood by the ratio of the flooded river reach to the total length of the river channel. Shi (2022) simplified the pipe system and river network in one dimension, with flows beyond the drainage capacity of the system entering the two-dimensional surface part through nodes, which is inconsistent with the actual process of river dike overtopping. Therefore, further research is needed on the complex physical process of compound floods in coastal areas with river networks.

Statistical models for the analysis of the dependence between flood driving factors are mainly used to estimate the likelihood of compound flood hazards, while numerical models provide key indicators for assessing flood risk in coastal regions, such as inundation depth and area (Xu et al., 2023). Therefore, to quantify the impact of various driving factors on compound floods, numerical simulation using hydrodynamic models is considered in this study. However, there are still some research gaps in this research domain. These include: (1) the majority of the current numerical modelling studies consider only two driving factors (rainfall and tides), which may be insufficient for some coastal cities as their floods can be affected by more factors, i.e., upstream river flows, downstream tidal levels and local rainfall intensity, (2) previous efforts mainly focus on the surface inundation in the estuary area or along the main single river affected by the combination of rainfall and tide, their modelling methods cannot be directly used to handle urban river networks with complex underlying hydraulic interactions in coastal cities.

The above deficiencies have been addressed in this work by focusing the work in this paper on the hydrodynamic processes and flooding risk in the plain coastal river network area that can be affected by all three driving factors (upstream river flows, downstream tidal levels and local rainfall intensity). When constructing the hydrodynamic model, this article also uses a two-dimensional method to integrate the river channels and land surface to ensure accuracy of the inundation simulation. Finally, when analyzing the flood risk, this work formulates and uses a series of scenarios to perform quantitative analysis for each of the three driving factors and the related compound effects.

It is noted that some frameworks have been proposed in recent years to analyze the compound flood risk. For example, Hsiao et al. (2021) developed a framework to investigate the compound flood risk induced by two driving factors (rainfall and tides) in a changing climate, and Qiang et al. (2021) proposed a framework driven by rainfall, tides and storm surges. In contrast, this paper proposes a framework to better understand the hydrodynamic processes and risk of compound flooding in coastal river floodplains, with driving factors being upstream river flows, downstream tides and local rainfall.

In this study, the coastal urban area (Qianshan River basin) of Zhuhai City in the Guangdong-Hong Kong-Macao Greater Bay Area (GBA) of China is applied as a typical example for the demonstration of this framework. Firstly, a hydrodynamic model is built to simulate the urban inundation of the region with the complex river network. In particular, upstream river flows, downstream tidal levels and local rainfall intensity are taken into account in the model to accurately simulate the complex flood mechanism of coastal cities. Then, based on the hydrodynamic model verified from observation data, the coastal flooding process and consequence of the focused case study are quantified and evaluated for the compound impacts of the river inflow, tidal level and rainfall intensity. In addition, the patterns of the joint occurrence between the rainfall and tidal peaks are considered in the proposed framework. Through the systematic analysis, the dominant influence factors and their compound effects are identified to formulate appropriate flooding reduction measures.

2. The modelling method

The proposed framework is shown in Fig. 1. Briefly, the framework consists of two components, namely, the setup of a comprehensive hydrodynamic model for a typical coastal urban drainage system, and the quantitative analysis of compound flooding consequences caused by multiple factors. The proposed framework can reproduce the coastal flooding dynamics and mechanism as well as quantify the flooding consequences, which are useful for coastal urban flood prevention and management. For clarity, each of these two components is elaborated as follows.

2.1. Hydrodynamic model

One of the keys to building an effective hydrodynamic model in this proposed framework (Fig. 1) is to comprehensively consider the multi-source factors that may lead to coastal compound floods. In practice, most coastal urban systems are located on the plain areas near the estuary at the lower reaches of river basins/networks to gain better water resources and convenient transportation, which is however usually low-lying and has complex flow systems (e.g., river, estuary, ocean). As a result, once extreme rainstorms occur, combined with sudden floods in

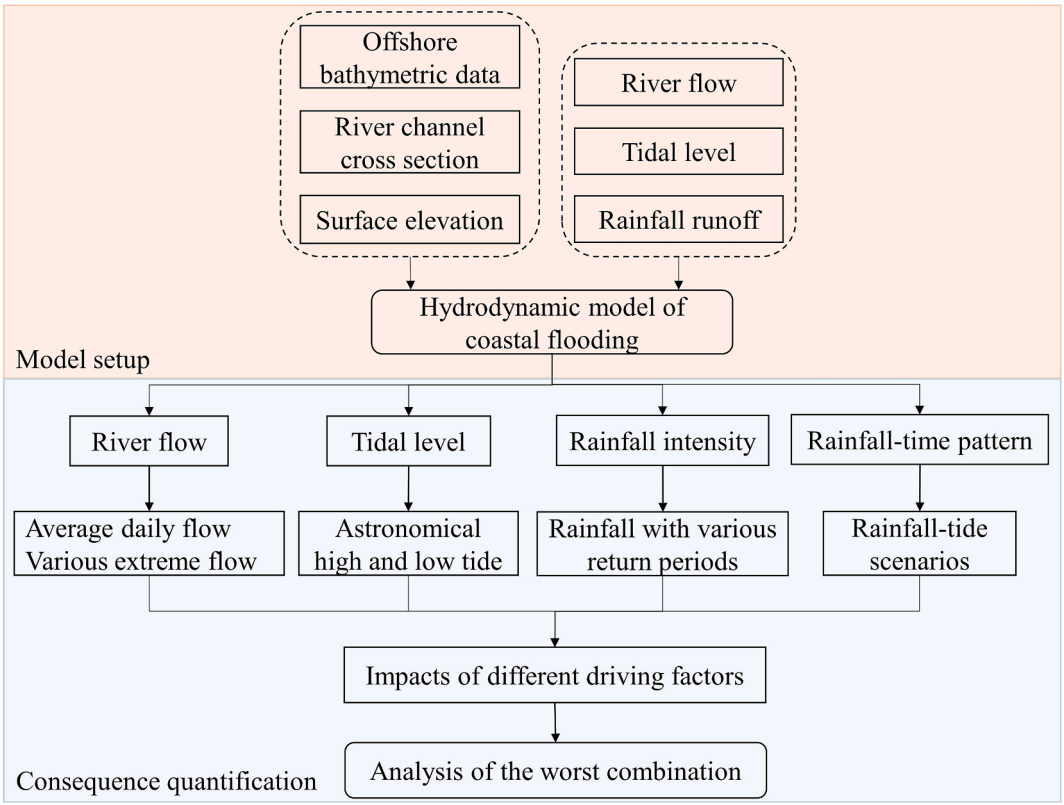

Fig. 1. The framework of hydrodynamic process simulation and consequence quantification of coastal compound flooding.

rivers and high tides in coastal waters, it is very easy and possible to cause unexpected drainage issues in the city or even backflow of seawater and river water, thereby causing serious flood disasters in a coastal urban system (Erikson et al., 2018). Therefore, to construct the hydrodynamic model of the river channels, it is necessary to expand the simulation scope of the model to include the river tributaries and the coastal ocean area linked to urban drainage systems. This can facilitate to accurately simulate overall dynamic processes and complete influence mechanisms of the coastal compound flooding induced by multi-source factors.

The framework proposed in this paper uses a two-dimensional (2D) model to achieve the required efficiency and accuracy for the simulation of coastal flooding. That is, when solving the Navier-Stokes equations for incompressible fluids, the vertical acceleration factor is not considered in the vertical momentum equation. For the internal rivers of coastal cities and the surrounding open sea, the horizontal motion scale is much larger than the vertical motion scale, so it is sufficiently accurate to use the vertical average method for improving the simulation efficiency. However, results can be more accurate than the one-dimensional (1D) model simulation because of the inclusion of the surface water flow effect. For this purpose, the Delft3D FLOW model developed by Deltares (2014) is selected to build a 2D hydrodynamic model of coastal drainage and flooding processes. The Delft3D model is a widely used hydrodynamic model that has been verified through various applications in the literature, with details given in Deltares (2014). It is also noted that the orthogonal body-fitted grid used in the Delft3D model can well adapt to the changes in terrain and boundaries, and the alternate implicit method used to solve the above equations presents relatively fast calculation speed and high stability (Lee et al., 2019). In this paper, this model is firstly calibrated and verified through observation data collected and then is used for extensive applications for coastal flooding simulation and analysis.

2.2. *Quantification of coastal compound flooding*

With the aid of the hydrodynamic model, a quantitative analysis of the multi-source driving factors is conducted to better understand the mechanism of coastal flooding and the importance of different influencing factors. Three factors, upstream river flows, tidal variations and rainfall intensity are analyzed in this study. The annual average daily flow and flows with different return period in the upstream river of the studied case (Zhuhai City) are estimated based on the historical data. Based on historical tidal level data, a typical high tide period and a typical low tide period are selected for analysis.

For the study region, the extreme rainfall with a two-hour duration is more likely to induce a larger flood risk compared to a longer rainfall duration (e.g., 24-hour) with the same return periods. This is because that this study region has a high river channel density, where the size of the sub-catchments associated with the river is quite small and hence the runoff time on the ground and in the pipe is relatively short. This also matches well with flood observations in this region provided by the local flooding authority, where flooding is often induced by short-time duration rainfall events in summer. Therefore, two-hour duration rainfall events with different return periods are used to simulate and analyze their impacts on urban floods, with analysis given in Section 4.2. In addition, the coastal flooding severity and consequence in the study region caused by different encountering scenarios of rainfall and tidal peaks are analyzed and quantified. After identifying the main drivers of local compound floods, the impact of the worst-case scenario is analyzed to highlight the characteristics of local floods.

3. Case study

The Qianshan River basin in Zhuhai City within the GBA of China is selected as the case study to enable the coastal compound flooding analysis. The hydrological and climatic characteristics of the study region, as well as the initiation and verification process of the established

hydrodynamic model, are introduced in detail below.

3.1. Study region

Regarding the geographical position, Zhuhai City is located on the west bank of the Pearl River estuary within the GBA of China, which is the only city on the mainland that is connected with Hong Kong and Macao simultaneously by land (bridge). For the studied region, Qianshan River is located in Zhongzhu Lianwei in the southwest of Xiangzhou District of Zhuhai City as shown in Fig. 2. Many inland rivers are interconnected in the region. For the drainage system, there are 73 large and small rivers and drainage channels in the basin, with a total length of about 200 km. Due to the special geographical location and topographic conditions, the Qianshan River basin often suffers from compound flood disasters caused by flows in the river (Modaomen waterway), high tidal levels and the local heavy rainfall runoffs.

The information required for the compound flood modeling and analysis includes terrain data in the basin, river network and offshore water depth data, rainfall conditions, river flows and tidal level records. The topographic data of the Qianshan River basin is retrieved from a 5 m × 5 m resolution digital elevation model (DEM) provided by the local surveying and mapping department. Nearshore water depth and coastline are extracted from the navigation chart (China Maritime Safety Administration, 2008). The cross-sections of each river in the basin are obtained by the local hydrological bureau through field surveying and mapping. Cross-sectional data are collected at an average distance of 100 m. As shown in Fig. 2(a), the rainfall data is recorded from the local ZXD Rainfall Station, the observed flow of Wuzhou Station in the upper reaches of the Xijiang River is selected as the flow of the outer river, and the tidal level observations of DHQ Station in the estuary is taken as the tidal level in the study region. In addition, the local rainfall with different return periods is determined according to the Zhuhai rainstorm intensity formula and calculation chart (nearly 50 years long) using the latest version of 2015.

3.2. Model assumptions

A number of assumptions are made in this study to enable the model development in this study, with details given below.

Assumption 1. *To ensure the stability of numerical modelling, the upstream boundary has to be set outside of the tidal boundary not to be affected by tidal waves. The resultant region of interest for the simulation is shown in Fig. 2b as suggested by the local flooding management authority. However, such a large region significantly increases the challenges for model development as it requires a large topographic data set which is often not available. To address the problem, following Huang et al. (2020), this paper uses the generalized channel model to simulate the flow from Tianhe Station to the upstream open boundary (the Wuzhou Station). This generalized river model has a total length of 280 km, with a width of 1,300 m, an average slope of 0.058 ‰ and an average water depth of 8 m (Huang et al., 2020). The accuracy of this model has been demonstrated by Huang et al. (2020) using field observations. In this study, the domain decomposition technology is used to divide the model grid into four parts from north to south (Fig. 2b), and decrease the river network area on both sides at the highest resolution (Fig. 2c) to reduce the simulation time. Meanwhile, Manning roughness coefficients can be set for each part based on its terrain characteristics to improve simulation accuracy.*

Assumption 2. *For this case study, the model establishment involves two boundaries: the upstream boundary represented by river flow of the Wuzhou Station, and the downstream boundary represented by tidal level of the DHQ Station (see Fig. 2). However, the model only contains the mainstream of the Modaomen waterway and Xijiang River but omits its branches, so a diversion coefficient needs to be set to exclude the flow shared by the branches. Given that the DHQ Station is the nearest hydrological station to the outer sea boundary of the model, tidal level observations of this station are considered as the downstream boundary. It is acknowledged that this may result in modelling errors, but these errors should be relatively small. This is because that this station is located at the entrance of Modaomen waterway, meaning that it measures the tidal levels of the open ocean surface and hence these observations can be considered as approximations to the tidal levels at the actual downstream boundary (the Part IV boundary). Nevertheless, future studies should endeavor to place monitoring stations at the actual downstream boundary to further improve the modelling accuracy.*

Assumption 3. *In this study, the surface runoff and the drainage pipe network are not involved in the simulation, because the detailed pipe information for the study region is not available. Such a simplification may overestimate the flooding risk as the runoff time on the ground and in the*

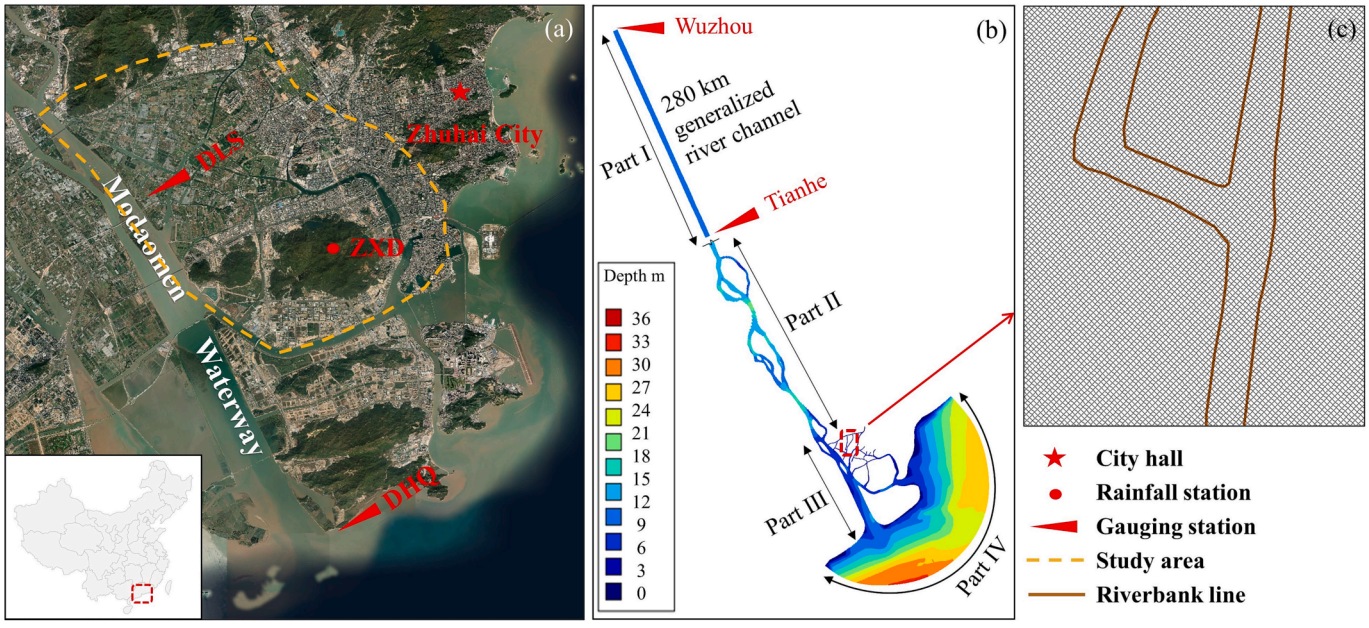

Fig. 2. (a) Location and layout of the study region in the Qianshan River basin in Zhuhai city; (b) Overview of the hydrodynamic river network model established in the Delft3D in the form of water depth; (c) The high-quality grid of a section of the river channel.

network pipes is ignored. However, given that the study region has a high river channel density, the drainage pipes are relatively short as many sub-catchments are near the river. Consequently, the runoff time on the ground and in the pipes are quite short and hence the ignorance of the runoff time would not significantly affect the flooding simulation results (with more discussion provided in Section 4.1). Therefore, in this study, the river channel is assumed to have many inflow points with an average interval of 1 km. Each inflow point is connected with a particular sub-catchment based on the elevation data, which is provided by the local flood management authority. The rainfall depth (5-minute rainfall duration) at each sub-catchment is directly converted to flows associated with its corresponding inflow point.

In this study, the water level and elevation take the Pearl River Base (the height) as the base line, and the water level at each mesh is set as 0 m at the initial time of the model. Therefore, while the water level of a grid is zero, it has a particular initial water depth as its corresponding ground may be below zero relative to the base line. This initial water depth at some grids can be used to initiate the model, followed by running the model using the upstream flows of the Modaomen waterway and the downstream tides as the inputs. According to the preliminary simulation tests, a 3-day cold start time is sufficient to ensure the water level simulation stable. Subsequent model verification and analysis only use the results within the next two days, so the total simulation duration of the model is set to 5 days. The rainfall inputs are only considered within the last two days.

3.3. Model calibration and validation

With the preliminary construction of the model, it is necessary to further determine the grid size of the river network area, the flow diversion coefficient of Wuzhou Station, the Manning coefficient of each region and the simulation time step through calibration. This process adopts a section of observation data from the 2020 flood season, and uses the daily highest and lowest water levels of DLS Station for three consecutive days as a reference. In the river network area, three grid resolutions of 25 m × 25 m, 10 m × 10 m and 5 m × 5 m were used for the simulations, and the grid resolution of 10 m × 10 m (Fig. 2c) was finally selected based on its good trade-off in simulation accuracy and computational efficiency.

When setting the diversion coefficient, this study uses 70 % based on observation data provided by the local water authority, and this diversion coefficient has been validated using simulation results in this study. After testing the Manning roughness coefficients of each region, it was found that selecting different values within their respective empirical range had little impact on the results. Therefore, the median values were taken to enable simulations. Finally, three time steps were tested, namely 15 s, 12 s, and 6 s, and it is found that 12 s is the maximum step size that the model can converge, and further reduction of the time step size has small effect on the water level results.

After defining the parameters above, two periods chosen from flood season are selected for the model validation, namely from May 19 to 23, 2020, and from May 29 to June 2, 2021, shown in Fig. 3. The rainfall is set according to the records of ZXD Rainfall Station, from which the total rainfall is 36 mm on May 22, 2020, and 267 mm on June 1, 2021. Due to the lack of sufficient observation data, this study takes the DLS Station as the verification location, which records measured water level values every 5 min.

It can be seen from Fig. 3, despite of some deviations, the simulation results of DLS station are overall similar to the observed data during these two periods of flow variations. The deviation of model simulation results mainly comes from the quality of datasets and the model assumptions. In this study, the root mean square error (RMSE) and the Nash coefficient (NSE) are used to evaluate the accuracy of the hydrodynamic model. The water level RMSE values between the simulations and observations under the two rainfall events are respectively 0.081 m and 0.120 m, and the NSE values are 0.958 and 0.941 respectively. This indicates that the developed model possesses acceptable accuracy, and hence it can accurately simulate the hydrodynamic process of the studied basin region.

4. Results and discussion

A series of scenarios are simulated using the 2D hydrodynamic model to explore the impacts of different factors, including the flows in the Modaomen waterway, tidal levels in the outer sea and the local rainfall intensity, as well as the rainfall-tide coincidence patterns on the coastal compound flooding in the Qianshan River basin. These scenarios are presented in Table 1.

The simulations use the tidal forcing during the local flood season, starting from 8:00 on May 28, 2021, lasting for 5 days. Different return periods for Modaomen flows and rainfall are considered and determined according to the needs of each simulation. The Water Security Plan for GBA issued by the Ministry of Water Resources of China emphasizes that by 2025, the local drainage standard should be higher than a 30-year return period, and by 2035 the flood control standard should not be lower than a 100-year return period. The average daily flow of the river (Modaomen waterway) is about 10,000 m^3/s, and the 2-year, 20-year and 50-year return period of the river flow values are 28,000 m^3/s, 47,000 m^3/s and 54,000 m^3/s respectively. The 54,000 m^3/s is the largest flow recorded (Liu et al., 2021; Chen et al., 2019).

Based on the local historical data and frequency analysis, the

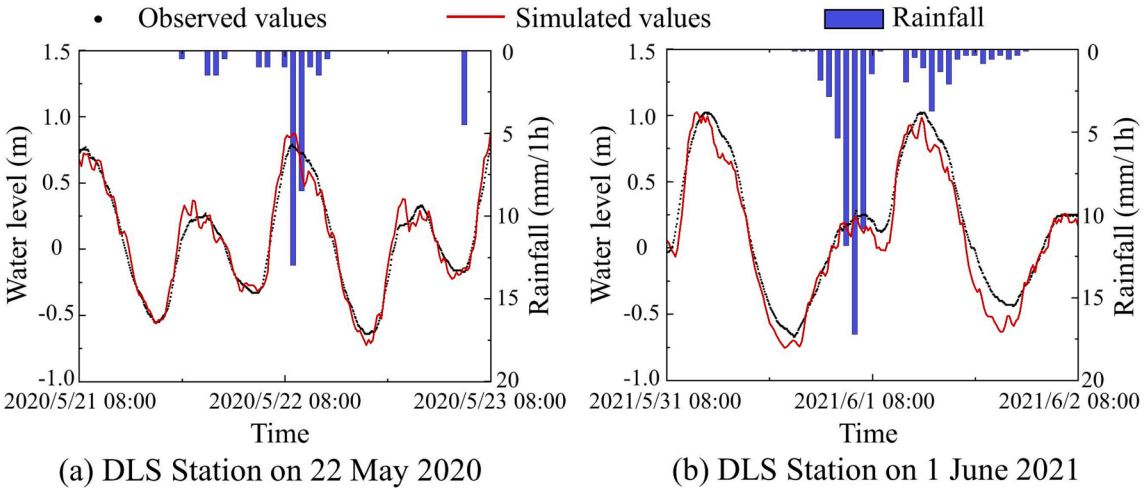

Fig. 3. Comparisons of the modelled and observed water levels at DLS Station from May 21 to May 23, 2020, and from May 31 to June 2, 2021.

Table 1
Scenarios considered for compound flooding analysis in Qianshan River basin of Zhuhai City, China.

Scenario ID	Upstream river flow (m^3/s)	Rainfall return period	Tide	Time interval between rain and tide peaks (min)[1]
A	Q = 10,000 Q = 28,000 Q = 47,000 Q = 54,000	R = 30-year	High tide	L = 0
B	Q = 10,000 Q = 54,000	R = 30-year	High and Low tide	
C	Q = 10,000 Q = 54,000	R = 5-year to 100-year	High tide	L = 0
D	Q = 10,000	R = 30-year	High tide	L = [−60, 90]

[1] The time interval of rainfall and tide peaks refers to the time of rainfall peak minus that of tide peak, i.e. positive value means that rainfall peak occurs later than tide peak and the opposite.

designed two-hour period rainfall varies from 125 mm (for a 5-year return period) to 233 mm (for a 100-year return period), and it is assumed that the rainfall peak and tide peak occur simultaneously to exhibit the greatest impact of the rainfall (Chen et al., 2020). In order to explore the impact of rainfall-tide coincidence on floods, the rainfall time is changed with an interval of 10 min to analyze whether there is an accurate worst-case scenario.

4.1. Impact of the runoff process

This section explores the impacts of the ignorance of the runoff process (ground and pipe) on the simulation results. Two simulation methods are conducted to enable the comparison: Method 1 used in the current study does not consider the surface runoff and pipe flow processes, and Method 2 takes the surface runoff and pipe flow into account. Given that the urban drainage pipe information is not available, Method 2 is implemented using the following strategy. Firstly, a runoff time is estimated based on the size and the slope of each sub-catchment. This runoff time represents the total time used for the surface runoff and pipe flow for each sub-catchment, ranging from 5 min to 1 h. This is followed by taking this runoff time as the delay time for each corresponding inflow point on the river.

Fig. 4 presents the results of Methods 1 and 2 under different scenarios. From this figure, it can be seen that the spatial distribution of the flooded area is similar between Methods 1 and 2. More specifically, the maximum flooded area of Method 1 is only 3.4 % larger than that of Method 2 under the two different scenarios. This implies that the simple method used in this paper (Method 1) is effective in representing the hydrodynamics of the flooding process, while having benefits for model development due to its simplicity.

4.2. Impact of different rainfall time periods

Fig. 5 shows the maximum flooded area for the case study using the two-hour and 24-hour rainfall events with the same 30-year return period, where all the other conditions are identical for these two events, including the upstream river flows and the downstream tidal levels. As shown in this figure, under the same rainfall return period, the flooding caused by the two-hour rainfall event is more severe than one caused by the 24-hour rainfall event. More specifically, the flooded area caused by the 24-hour duration rainfall is 11.32 km^2, which is significantly lower than that caused by the two-hour rainfall event with the flooded area of 20.58 km^2. Similar observations are made when using other boundary conditions and hence results are not presented. This implies that for this region with a high river density, the use of rainfall events with a short duration can be more realistic to represent the underlying flooding risk.

4.3. Influence of river flows on flooding

The first flood-driven factor considered is the flows of the river (Modaomen waterway) through the coastal city and eventually into the

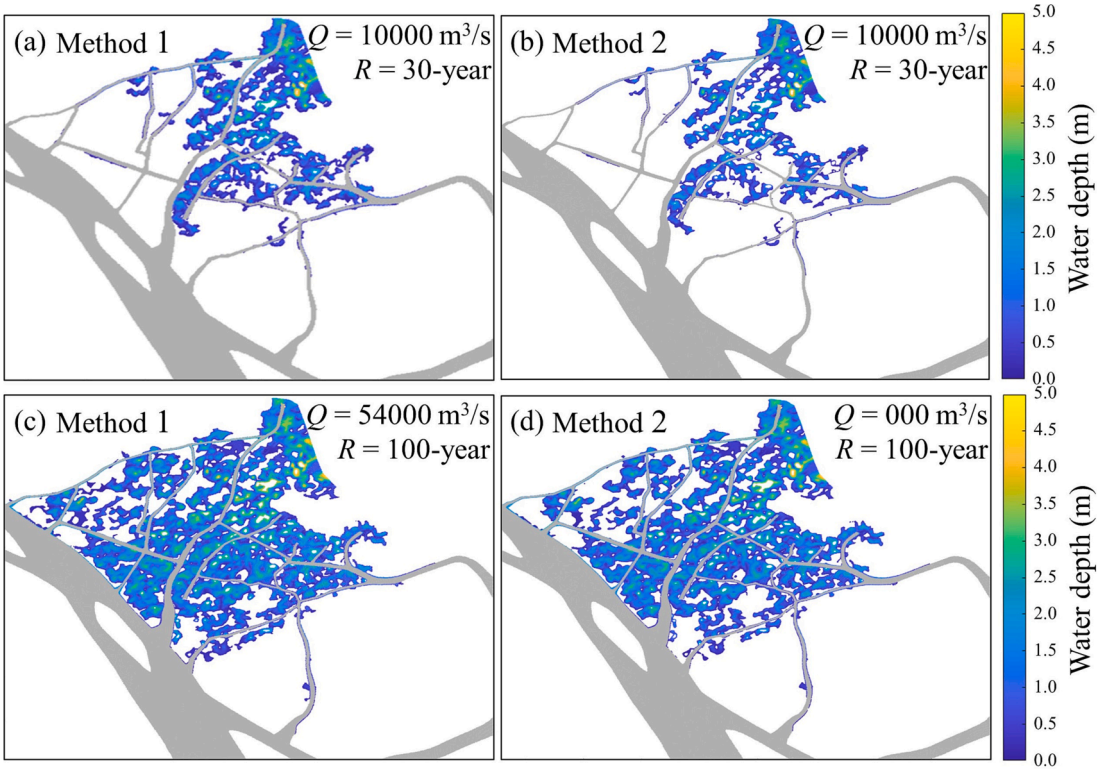

Fig. 4. The maximum flooded area of the study region. Method 1 does not consider surface runoff and pipe flow processes, and Method 2 takes them into account.

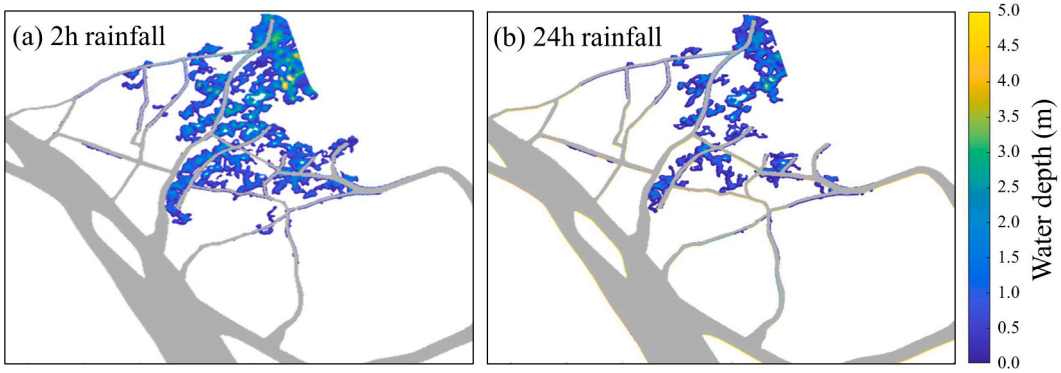

Fig. 5. The maximum flooded area using different rainfall duration events with the same return period under the same upstream flow and tidal level conditions.

outer sea. Four flow values are selected for simulation (scenario type A in Table 1) to analyze the impact of different river flows on compound flooding. Fig. 6 shows the maximum flooded area (Fig. 6a, 6b, 6c, 6d), the time evolution curves of regional flooded area (Fig. 6e) and the average river water level (Fig. 6f) for these four scenarios. Specifically, under the same rainfall and tidal conditions, when Q = 28,000 m^3/s in the Modaomen waterway, the flooded area increases by 4 km^2 (only about 2 % of the entire watershed area) compared to the general situation with Q = 10,000 m^3/s. While encountering a high flow of the Modaomen waterway, the flooded area increases sharply, which is 2.0

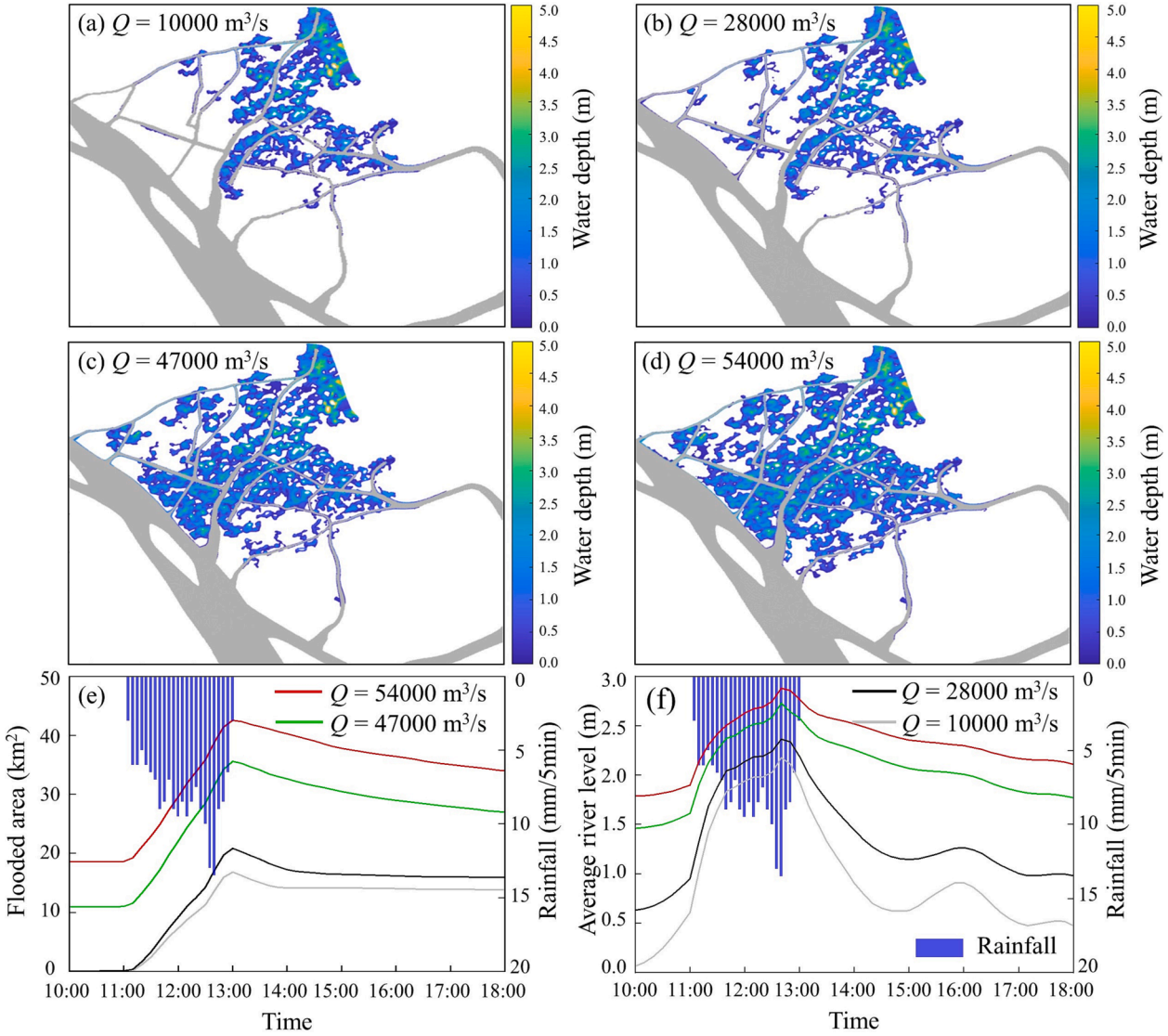

Fig. 6. The maximum flooded area of the study region and variation of the flooded area and average river level with time caused by different Modaomen flows. Q is the Modaomen flow; the average river level is obtained by calculating the real-time water levels of 26 monitoring locations uniformly distributed in the river network system of the study region.

times ($Q = 47{,}000\ m^3/s$) and 2.5 times ($Q = 54{,}000\ m^3/s$) of the general situation ($Q = 10{,}000\ m^3/s$).

As shown in Fig. 6e, when $Q = 10{,}000\ m^3/s$ and $Q = 28{,}000\ m^3/s$, floods occur after the start of the short duration rainstorm (i.e. 11:00 on June 1), while for high upstream flow ($Q = 47{,}000\ m^3/s$ and $Q = 54{,}000\ m^3/s$), there is a certain degree of inundation before rainfall, with the flood situation various depending on the river flow. Moreover, all the curves gradually stabilize after the rainfall but do not return to zero. This is because that with the ignorance of the drainage pipe system, the accumulated water on land caused by river flooding still exists in low-lying places after the water level drops, instead of fully returning to the river.

Fundamentally, this water area is influenced by both upstream flows and downstream tidal levels. For these four scenarios, the increase in flows can allow more water flow into the waterway, while the jacking effect of the downstream tidal levels remains unchanged. Therefore, the increased water flow accumulates in the study region and raise the water level of the whole area (as shown in Fig. 6f). Especially, the curves of scenarios for $Q = 47{,}000\ m^3/s$ and $Q = 54{,}000\ m^3/s$ show that the average river level has exceeded 1.5 m before the rain, and the elevation of the embankment top for the river network system is mostly 1.5–2.0 m. In summary, the compound flooding in the study region is greatly affected by the flow of the Modaomen waterway. This implies that the river flow can be an important influencing factor that induce floods in the study region. Therefore, controlling the upstream river flow through reservoirs can be an effective strategy to reduce the compound floods in the case study region.

4.4. Influence of coastal tidal levels on flooding

Scenario type B in Table 1 is designed to analyze the impact of astronomical tides on induced flood results, and the inundation situation is plotted in Fig. 7. From this figure, it can be seen that, compared to the low tide scenarios, the high tide scenarios can lead to more severe flooding, increasing the flooded area by approximately 8 km^2 (both for low and high Modaomen river flow). Although the flooded area varies under different flow conditions of the Modaomen waterway, the impact of tidal changes is similar. Therefore, the following is a further analysis of the flooding process under the low Modaomen flow (Q = 10,000 m3/s). Fig. 8a and 8b illustrate the time-varying curves of flooded area and volume for these different tide scenarios. The similarity of the two figures shows that the inundation process changes synchronously in terms of area and volume. This is because the surrounding area where the water first overflows the river embankment is relatively flat, and the high ground areas (that can prevent flood spreading) are mainly located downstream of the river network, i.e. in the south of the basin (as shown in Fig. 2a).

Meanwhile, Fig. 8c shows that when compound flooding occurs during the low tide period, the average water level in the river network area is generally below 1.5 m, while during the high tide period, the water level is between 1.5 and 2.0 m, which indirectly reflects that high tidal levels are more likely to cause local floods. In addition, Fig. 8d illustrates the changes in drainage capacity of the region. After the flood occurs, when comparing the inflow of the river network during the high tide period (800 m^3/s) and the outflow during the low tide period (300 m^3/s), the short-duration heavy rainfall could make the area quickly become an outflow state, and the solid and dashed lines begin to approach. The regional drainage capacity gradually offsets the impact of the tidal level and is dominated by rainfall. Finally, these results and comparisons in Fig. 7 and Fig. 8 indicate that although the impact of the astronomical tide is limited, it is necessary to consider the deteriorating effect of high tidal levels on flood process and consequence when studying compound flooding in coastal areas.

4.5. Influence of rainfall return periods on flooding

According to scenario type C in Table 1, simulations are conducted for different rainfall scenarios with different return periods (5-year to 100-year). Fig. 9a shows the variation curve of the maximum flooded area caused by different rainfall events under different upstream river flow conditions (Q = 10,000 m^3/s and Q = 54,000 m^3/s). As it can be seen from this figure, with the rainfall intensity increasing (with an increased return period), the flooded area of this region expands significantly. For low river flow (Q = 10,000 m3/s), the flooded area of 100-year return period rainfall is approximately three times that of a 5-year return period rainfall; For high river flow (Q = 54,000 m^3/s) as shown in Fig. 9a, the difference in maximum flooded area over different rainfall return periods is still large.

In addition, the combined effects of tidal levels and rainfall frequency/intensities are analyzed in Fig. 9b (taking low river flow Q =

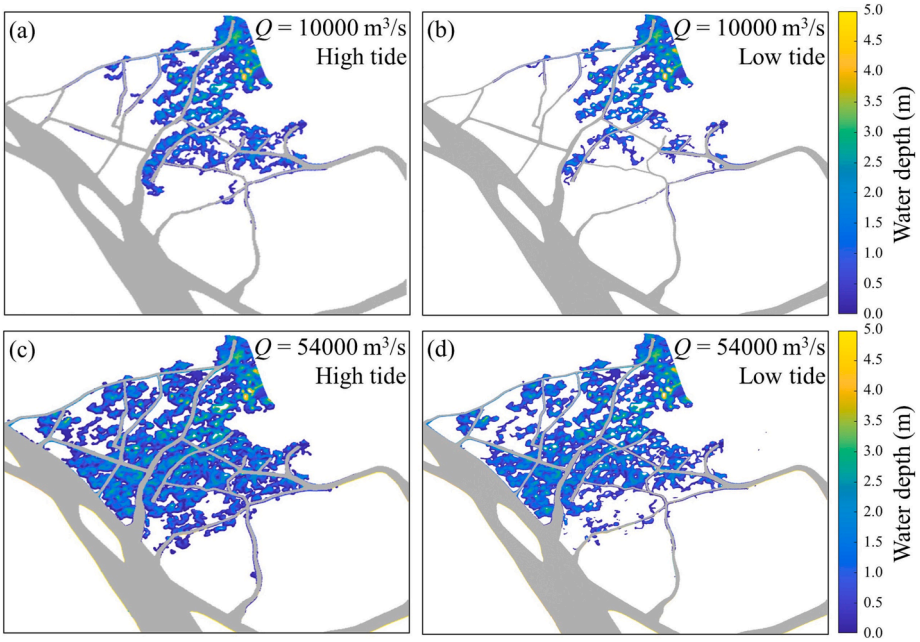

Fig. 7. The maximum flooded area in the study region under different astronomical tidal levels.

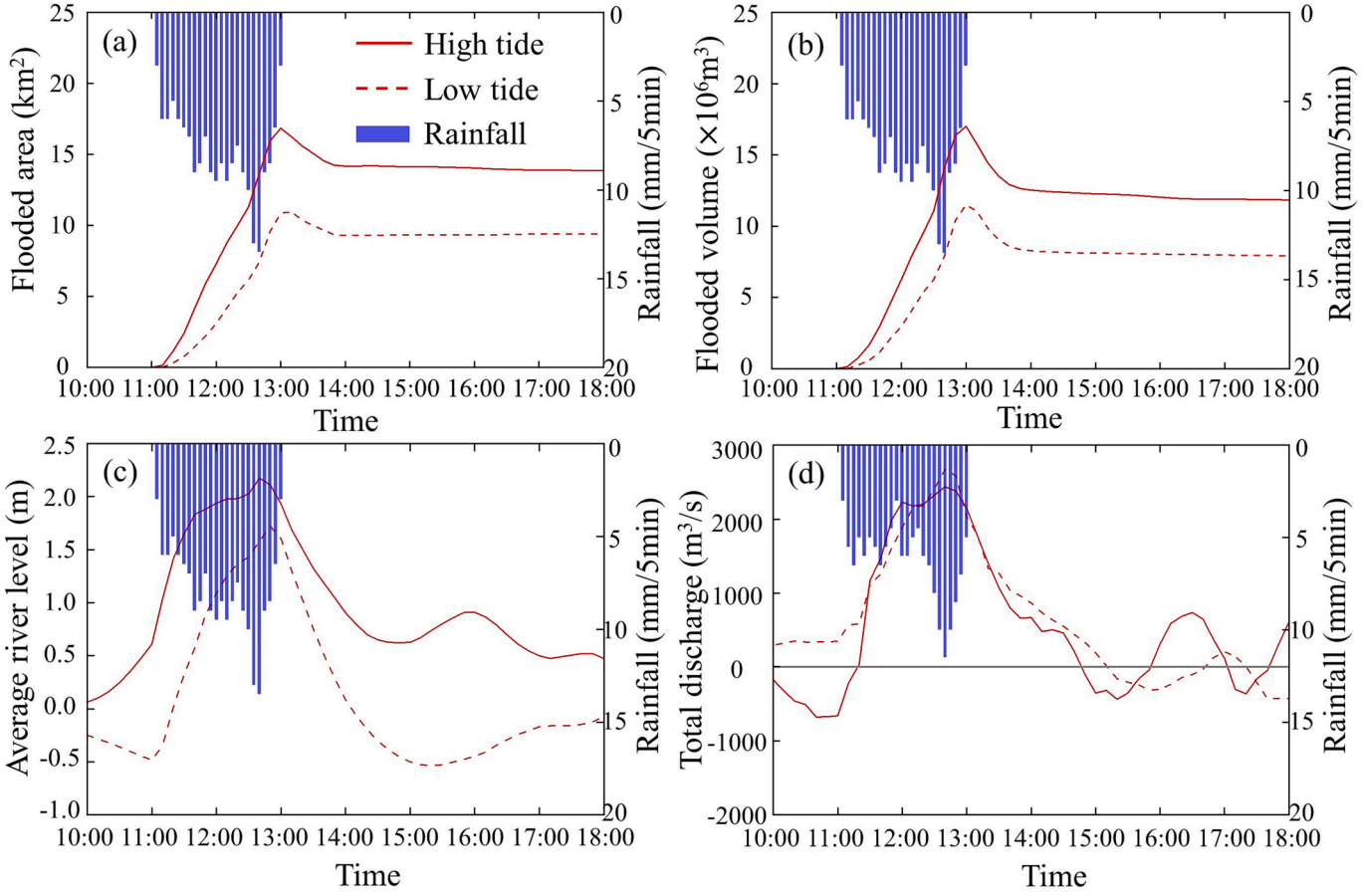

Fig. 8. Flooding process for low Modaomen flow under different astronomical tidal levels: (a) flooded area; (b) flooded volume; (c) mean water levels of the river network; (d) total river discharge of the river network.

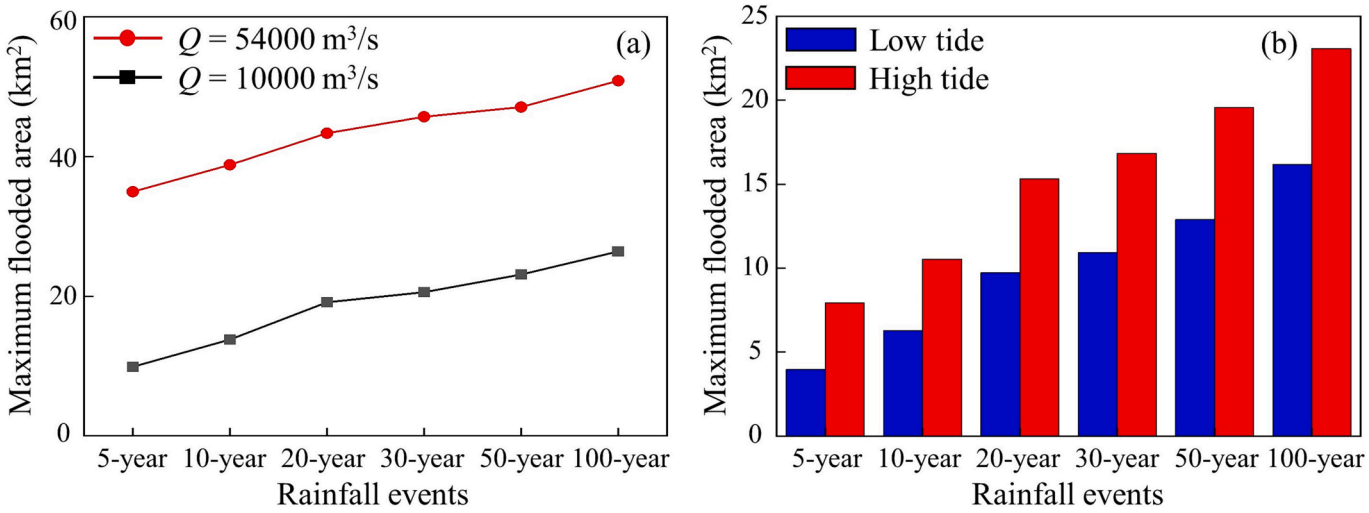

Fig. 9. (a) The variation of the maximum flooded area with time caused by different rainfall intensities; (b) The maximum flooded area for different rainfall intensities and tidal levels.

10,000 m^3/s as an example). Through simple calculations it can be obtained that under the high tide scenarios, the average change of the flooded area with rainfall intensity is about 10 %, while in the low tide period, it is around 13 %. Therefore, based on the results obtained, it can be concluded that rainfall intensity has a more significant and direct impact on the extent of flooding and related consequences in the analyzed coastal urban region.

4.6. *Influence of rainfall-tide coincidence on flooding*

When exploring the impact of rainfall-tide coincidence on flooding, for clarity, Fig. 10a only depicts the time-varying curves of the flooded area in the study region under several scenarios of scenario type D in Table 1. Different encountering scenarios in a short period of time mainly change the beginning and end moment of the flood due to

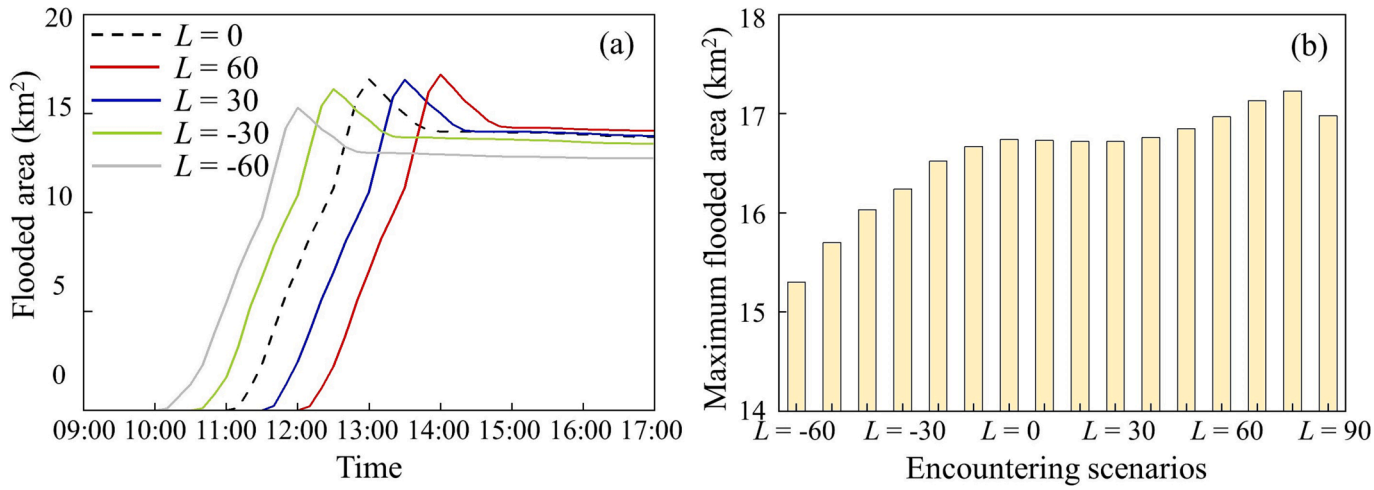

Fig. 10. Flooding process and consequence in the study region under different rainfall-tide encountering scenarios: (a) the flooded area for different peak interleaving times; (b) maximum flooded area of 16 different rainfall-tide encountering scenarios.

differences in rainfall occurrence time, but have little impact on the evolution characteristics of the flood. Specially, Fig. 10c displays the maximum flooded area for all 16 scenarios ($L = [-60,90]$), and the results demonstrate that the simultaneous occurrence of rainfall and tide peaks ($L = 0$) is not the worst case for flooding. This is because that although the maximum flooded area is generally positively correlated with the average tidal level values, during a two-hour rainfall period, there is not much change in the downstream tidal level. Moreover, the difference in flooding results between the worst scenario ($L = 80$) and the co-occurrence scenario ($L = 0$) is less than 1 km^2. Overall, the flooding extent of this region is relatively insensitive to the changes in the timing of high tide and rainfall coinciding within a short period.

4.7. Analysis of compound effects on flooding

In addition to the impacts of each of the above-mentioned driving factors, the combined (i.e. compound) effects of these factors could potentially intensify the flooding, as demonstrated in previous studies (Zheng et al., 2017; Shi et al., 2022). Here, based on the above analysis and results, the compound flood effects of the most extreme combination are analyzed. In particular, it is assumed that the 50-year return period river flow, the high tide and the 100-year return period rainfall occur

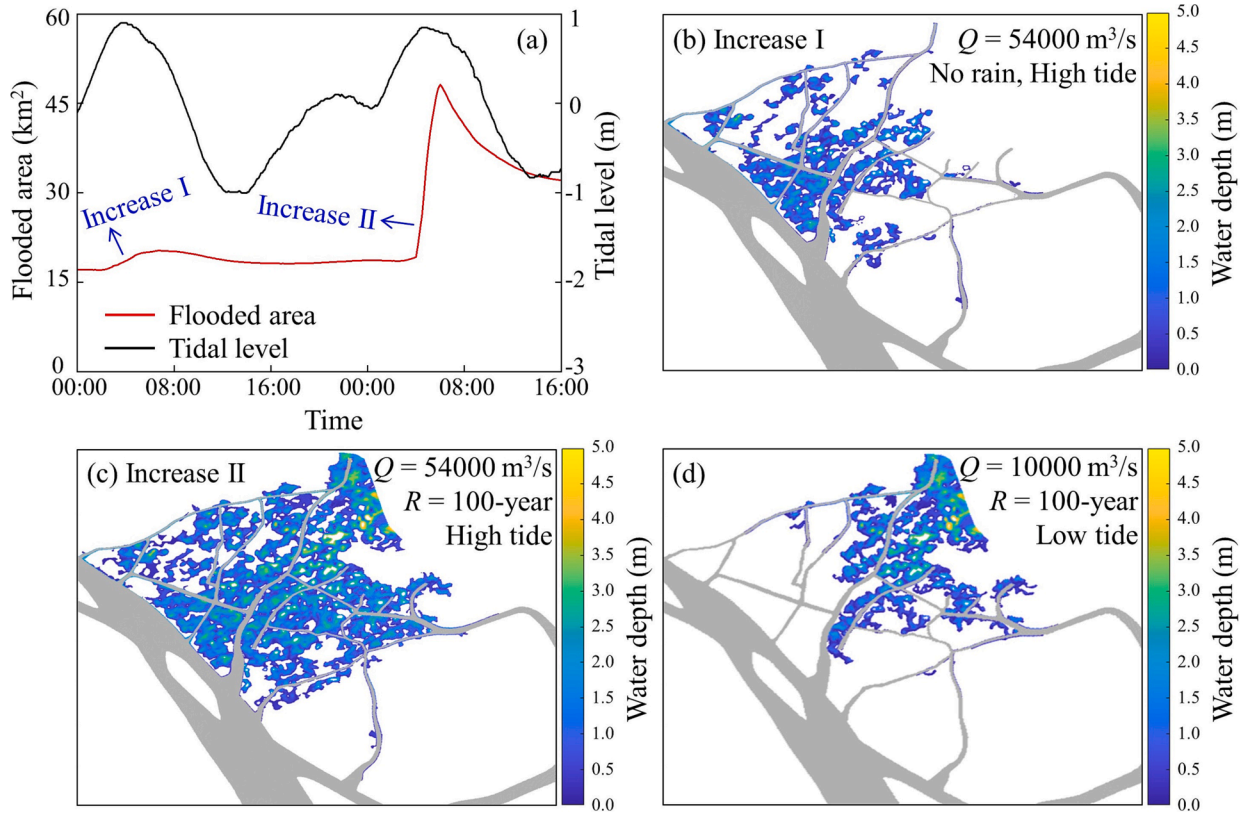

Fig. 11. (a) The time-varying curve of the flooded area for the most extreme compound flooding; The maximum flooded area for (b) Increase I, (c) Increase II, and (d) the rainfall dominated scenario.

simultaneously.

In this scenario, prior to the occurrence of rainfall, the water level in the study region is mainly determined by upstream Modaomen flow and downstream tidal level. When the extreme river flow (the 50-year return period river flow) encounters the high tide, the water level in the ocean can be significantly higher than that in the river network. This forces the ocean water flowing into the study region and hence causes local floods. When a short duration rainfall subsequently occurs, the river flow in urban land areas increases rapidly due to the strong impediment of the high water level in the ocean. Consequently, a serious urban flooding event occurs for such a worst scenario.

Specifically, Fig. 11a shows the long-time variation curve of flooded area under the most extreme scenario. There are two flooding events (Increase I and Increase II) during this period, with the maximum flooded area throughout these processes shown in Fig. 11b and 11c. It can be concluded that local floods can be extremely severe in this scenario (Increase II). The flooding level develops rapidly in a short period of time, ultimately causing nearly 50 km^2 of areas to be inundated, with an average flooded depth of 1.3 m. More specifically, the flooding region covers over 80 % of the central plain of the study region, while some downstream locations have also emerged with higher water depths.

In addition, the small peak in the flooded area before rainfall indicates that under the 50-year return period Modaomen flow, only combining with the downstream high tide would cause flooding of about 20 km^2. Fig. 11b with 11d show that floods dominated by different factors have different characteristics. When the combination of river flood and high tide occurs, the water level of the external water body significantly rises, and the inundation mainly occurs in the area near the Modaomen waterway. When the main flood-driven factor is only the 100-year return period rainfall, the flooded area is mainly occurring in the upstream parts of the basin. The difference in flood extent clearly indicates the necessity to study the multi-source induced flooding in coastal areas. One important contribution of this study is additional insights into the compound effects of different factors and the characteristics of flooding-prone areas, which is necessary to provide targeted local flood prevention measures.

5. Summary and conclusions

In this study, a framework has been developed for reproducing the coastal flooding dynamics and quantifying the flooding consequences under multiple scenarios that involves different flood-risk drivers (river flow, tidal level, and short-duration rainfall). A two-dimensional hydrodynamic model is developed using the Delft3D software to simulate and analyze the compound flooding of the coastal area of Zhuhai City in the Qianshan River basin of China. This 2D hydrodynamic model has been calibrated and validated using the available observation data. The developed model is accurate and efficient in capturing the drainage flow variations and induced flooding in the region. The validated model is applied to study the effect of several influencing factors and their relative importance on coastal urban flooding under different drainage and rainfall scenarios. The main results and findings from the analyzed case study can be summarized as follows:

(1) The framework is capable of revealing effectively the complex relationship between the upstream river flow, the tidal level and the local rainfall intensity as driving factors to contribute the compound flooding risk in the study region. Among these driving factors, local rainfall intensity shows the largest impacts on the flooding levels of the study region, followed by the upstream river flow. This implies that the construction of the rainfall retention tanks, development of the sponge cities in this region and control of the upstream river flows through reservoirs can be effective in managing the compound floods in this study region.
(2) The framework provides additional specific information that can be critical to guide the development of flooding control strategy in the analyzed case study. More specifically, the framework provides the flooding characteristics of different combinations of driving factors with varying return periods for the analyzed case study. For example, when a 50-year return period upstream river flow co-occurs with high tide and a 100-year return period rainfall, the resultant flooded area can be up to 50 km^2 for the study region, with an average of 1.3 m flooded depth. This information can then be used to more effectively control the flooding in this region.
(3) Regarding the impact of rainfall-tide coincidence effects (peak time) on flooding, the results obtained demonstrate that the maximum flooded area is positively correlated with the average tidal level during the two-hour rainstorm period, but the difference of flooded area between the worst case and the rainfall-tide coincidence scenario is less than 1 km^2. Therefore, it can be deduced that the influence of the time lag between short-duration rain and high tide is negligible for this study region.

The results and findings of this study are useful to understand the impacts of different factors and their compound effects on the coastal urban flooding process in the region studied in this paper. On this basis, relevant measures and procedures for coastal urban flood mitigation and management could be developed in advance for this coastal region. While the conclusion of this study is based on the Qianshan River Basin, the methodology and framework presented in this paper can be applied to other coastal city regions.

It is acknowledged that this study has two main limitations, which need to be considered in future studies. These are the ignorance of the impact of urban drainage network due to the lack of the pipe data, and a lack of a general quantitative framework for the compound flooding analysis. Furthermore, it is also noted that, due to the complexities and uncertainties of realistic rainfall events and coastal drainage conditions, more scenario applications (e.g., extreme weather and climate change) and additional analysis methods (e.g., intelligent data-driven models) should be implemented and coupled with the developed analysis framework in this study, which deserves further investigations in future.

CRediT authorship contribution statement

Jiao Yuan: Conceptualization, Methodology, Data curation, Software, Investigation, Writing – original draft, Visualization. **Feifei Zheng:** Conceptualization, Methodology, Writing – review & editing, Funding acquisition, Supervision. **Huan-Feng Duan:** Methodology, Writing – review & editing. **Zhengzhi Deng:** Conceptualization, Methodology. **Zoran Kapelan:** Methodology, Writing – review & editing. **Dragan Savic:** Methodology, Writing – review & editing. **Tan Shao:** Resources, Data curation. **Wei-Min Huang:** Resources, Data curation. **Tongtiegang Zhao:** Methodology, Writing – review & editing. **Xiaohong Chen:** Methodology, Writing – review & editing.

Declaration of competing interest

The authors declare that they have no known competing financial interests or personal relationships that could have appeared to influence the work reported in this paper.

Data availability

Data will be made available on request.

Acknowledgements

This work was supported by the National Key R&D Program of China (Grant No. 2022YFC3200032), NSFC-RGC Joint Research Scheme (JRS) under project (52261160379, N_PolyU599/22) and National Natural Science Foundation of China (NSFC, 52179080).

References

Administration, C.M.S., 2008. Macau Gang to Zhuhai Gang. China Navigation Publications Press, Tianjin.

Bermudez, M., Farfan, J.F., Willems, P., Cea, L., 2021. Assessing the effects of climate change on compound flooding in coastal river areas. Water Resour. Res. 57 (10) https://doi.org/10.1029/2020wr029321.

Bevacqua, E., Maraun, D., Haff, I.H., Widmann, M., Vrac, M., 2017. Multivariate statistical modelling of compound events via pair-copula constructions: analysis of floods in Ravenna (Italy). Hydrol. Earth Syst. Sci. 21 (6), 2701–2723. https://doi.org/10.5194/hess-21-2701-2017.

Bevacqua, E., Vousdoukas, M.I., Shepherd, T.G., Vrac, M., 2020. Brief communication: The role of using precipitation or river discharge data when assessing global coastal compound flooding. Nat. Hazards Earth Syst. Sci. 20 (6), 1765–1782. https://doi.org/10.5194/nhess-20-1765-2020.

Bilskie, M.V., Hagen, S.C., 2018. Defining flood zone transitions in low-gradient coastal regions. Geophys. Res. Lett. 45 (6), 2761–2770. https://doi.org/10.1002/2018gl077524.

Chen, W.J., Huang, G.R., Zhang, H., Wang, W.Q., 2018. Urban inundation response to rainstorm patterns with a coupled hydrodynamic model: a case study in Haidian Island, China. J. Hydrol. 564, 1022–1035. https://doi.org/10.1016/j.jhydrol.2018.07.069.

Chen, L., Teng, X., Pan, Z., Liu, W., 2019. Composition and encountering law of floods at Wuzhou station from main stream and tributaries in Xijiang River Basin. J. China Hydrol. 39 (6), 80–84.

Couasnon, A., et al., 2020. Measuring compound flood potential from river discharge and storm surge extremes at the global scale. Nat. Hazards Earth Syst. Sci. 20 (2), 489–504. https://doi.org/10.5194/nhess-20-489-2020.

Dash, P., Punia, M., 2019. Governance and disaster: analysis of land use policy with reference to Uttarakhand flood 2013, India. Int. J. Disaster Risk Reduct. 36 https://doi.org/10.1016/j.ijdrr.2019.101090.

Deltares, 2014. Delft3D-FLOW User Manual: Simulation of Multi-Dimensional Hydrodynamic Flows and Transport Phenomena, Including Sediments. pp. 686 Technical report. Version: 3.15, Revision 36209.

Eilander, D., et al., 2020. The effect of surge on riverine flood hazard and impact in deltas globally. Environ. Res. Lett. 15 (10) https://doi.org/10.1088/1748-9326/ab8ca6.

Erikson, L.H., O'Neill, A.C., Barnard, P.L., 2018. Estimating fluvial discharges coincident with 21st century coastal storms modeled with CoSMoS. J. Coast. Res. 791–795 https://doi.org/10.2112/si85-159.1.

Fang, J.Y., et al., 2021. Compound flood potential from storm surge and heavy precipitation in coastal China: dependence, drivers, and impacts. Hydrol. Earth Syst. Sci. 25 (8), 4403–4416. https://doi.org/10.5194/hess-25-4403-2021.

Gran Castro, J.A., Ramos De Robles, S.L., 2019. Climate change and flood risk: vulnerability assessment in an urban poor community in Mexico. Environ. Urban. 31 (1), 75–92. https://doi.org/10.1177/0956247819827850.

Hsiao, S.-C., et al., 2021. Flood risk influenced by the compound effect of storm surge and rainfall under climate change for low-lying coastal areas. Sci. Total Environ. 764 https://doi.org/10.1016/j.scitotenv.2020.144439.

Huang, S., Yin, X., Zeng, Y., Zhao, X., Ren, J., 2020. Study on correlation of factors affecting saline intrusion length in Modaomen estuary based on field observations. J. Hydroelectric Eng. 39 (8), 112–120.

Jane, R., Cadavid, L., Obeysekera, J., Wahl, T., 2020. Multivariate statistical modelling of the drivers of compound flood events in south Florida. Nat. Hazards Earth Syst. Sci. 20 (10), 2681–2699. https://doi.org/10.5194/nhess-20-2681-2020.

Kumbier, K., Carvalho, R.C., Vafeidis, A.T., Woodroffe, C.D., 2018. Investigating compound flooding in an estuary using hydrodynamic modelling: a case study from the Shoalhaven River, Australia. Nat. Hazards Earth Syst. Sci. 18 (2), 463–477. https://doi.org/10.5194/nhess-18-463-2018.

Lee, C., Hwang, S., Do, K., Son, S., 2019. Increasing flood risk due to river runoff in the estuarine area during a storm landfall. Estuar. Coast. Shelf Sci. 221, 104–118. https://doi.org/10.1016/j.ecss.2019.03.021.

Li, Z.M., Zhang, X.X., Ma, Y.F., Feng, C.Y., Hajiyev, A., 2019. A multi-criteria decision making method for urban flood resilience evaluation with hybrid uncertainties. Int. J. Disaster Risk Reduct. 36, 12. https://doi.org/10.1016/j.ijdrr.2019.101140.

Lian, J.J., Xu, K., Ma, C., 2013. Joint impact of rainfall and tidal level on flood risk in a coastal city with a complex river network: a case study of Fuzhou City, China. Hydrol. Earth Syst. Sci. 17 (2), 679–689. https://doi.org/10.5194/hess-17-679-2013.

Lian, J.J., Xu, H.S., Xu, K., Ma, C., 2017. Optimal management of the flooding risk caused by the joint occurrence of extreme rainfall and high tide level in a coastal city. Nat. Hazards 89 (1), 183–200. https://doi.org/10.1007/s11069-017-2958-4.

Liu, Z., et al., 2020. Cross-scale modeling of storm surge, tide, and inundation in Mid-Atlantic Bight and New York City during Hurricane Sandy, 2012. Estuar. Coast. Shelf Sci. 233 https://doi.org/10.1016/j.ecss.2019.106544.

Liu, Z., Wang, S., Cai, Y., Lan, F., 2021. Coincidence rules of rainfall in waterlogging area of tide-affected area and upstream flood in flood area of drainage receiver. Water Resour. Protect., 37(2): 89–94,107.

Moftakhari, H.R., Salvadori, G., AghaKouchak, A., Sanders, B.F., Matthew, R.A., 2017. Compounding effects of sea level rise and fluvial flooding. PNAS 114 (37), 9785–9790. https://doi.org/10.1073/pnas.1620325114.

Moftakhari, H., Schubert, J.E., AghaKouchak, A., Matthew, R.A., Sanders, B.F., 2019. Linking statistical and hydrodynamic modeling for compound flood hazard assessment in tidal channels and estuaries. Adv. Water Resour. 128, 28–38. https://doi.org/10.1016/j.advwatres.2019.04.009.

Nakamura, R., Mall, M., Shibayama, T., 2019. Street-scale storm surge load impact assessment using fine-resolution numerical modelling: a case study from Nemuro, Japan. Nat. Hazards 99 (1), 391–422. https://doi.org/10.1007/s11069-019-03746-6.

Qi, W.C., et al., 2021. A review on applications of urban flood models in flood mitigation strategies. Nat. Hazards 108 (1), 31–62. https://doi.org/10.1007/s11069-021-04715-8.

Qiang, Y., et al., 2021. Urban flood analysis for Pearl River Delta cities using an equivalent drainage method upon combined rainfall-high tide-storm surge events. J. Hydrol. 597 https://doi.org/10.1016/j.jhydrol.2021.126293.

Rey, A.J.M., Corbett, D.R., Mulligan, R.P., 2020. Impacts of hurricane winds and precipitation on hydrodynamics in a back-barrier estuary. J. Geophys. Res. Oceans 125 (12). https://doi.org/10.1029/2020jc016483.

Shen, Y.W., Morsy, M.M., Huxley, C., Tahvildari, N., Goodall, J.L., 2019. Flood risk assessment and increased resilience for coastal urban watersheds under the combined impact of storm tide and heavy rainfall. J. Hydrol. 579 https://doi.org/10.1016/j.jhydrol.2019.124159.

Shi, S.Y., Yang, B., Jiang, W.S., 2022. Numerical simulations of compound flooding caused by storm surge and heavy rain with the presence of urban drainage system, coastal dam and tide gates: A case study of Xiangshan, China. Coastal Eng. 172 https://doi.org/10.1016/j.coastaleng.2021.104064.

United Nations Regional Information Centre for Western Europe. (2022, March 14). Blue Economy: oceans as the next great economic frontier. https://unric.org/en/blue-economy-oceans-as-the-next-great-economic-frontier/.

Valle-Levinson, A., Olabarrieta, M., Heilman, L., 2020. Compound flooding in Houston-Galveston Bay during Hurricane Harvey. Sci. Total Environ. 747 https://doi.org/10.1016/j.scitotenv.2020.141272.

Wahl, T., Jain, S., Bender, J., Meyers, S.D., Luther, M.E., 2015. Increasing risk of compound flooding from storm surge and rainfall for major US cities. Nat. Clim. Change 5 (12), 1093. https://doi.org/10.1038/nclimate2736.

Ward, P.J., et al., 2018. Dependence between high sea-level and high river discharge increases flood hazard in global deltas and estuaries. Environ. Res. Lett. 13 (8) https://doi.org/10.1088/1748-9326/aad400.

World Meteorological Organization. (2021, August 31). Weather-related disasters increase over past 50 years, causing more damage but fewer deaths. https://public.wmo.int/en/media/press-release/weather-related-disasters-increase-over-past-50-years-causing-more-damage-fewer.

Xu, K., Wang, C., Bin, L., 2023. Compound flood models in coastal areas: a review of methods and uncertainty analysis. Nat. Hazards 116 (1), 469–496. https://doi.org/10.1007/s11069-022-05683-3.

Zheng, F., Westra, S., Sisson, S.A., 2013. Quantifying the dependence between extreme rainfall and storm surge in the coastal zone. J. Hydrol. 505, 172–187. https://doi.org/10.1016/j.jhydrol.2013.09.054.

Zheng, F., Leonard, M., Westra, S., 2017. Application of the design variable method to estimate coastal flood risk. J. Flood Risk Manage. 10 (4), 522–534. https://doi.org/10.1111/jfr3.12180.

Zscheischler, J., et al., 2018. Future climate risk from compound events. Nat. Clim. Chang. 8 (6), 469–477. https://doi.org/10.1038/s41558-018-0156-3.